

Observation of gamma-rays greater than 10 TeV from Markarian 421

K. Okumura¹, A. Asahara², G.V. Bicknell³, P.G. Edwards⁴, R. Enomoto¹, S. Gunji⁵,
S. Hara^{2,6}, T. Hara⁷, S. Hayashi⁸, C. Itoh⁹, S. Kabuki¹, F. Kajino⁸, H. Katagiri¹,
J. Kataoka⁶, A. Kawachi¹, T. Kifune¹⁰, H. Kubo², J. Kushida^{2,6}, S. Maeda⁸, A. Maeshiro⁸,
Y. Matsubara¹¹, Y. Mizumoto¹², M. Mori¹, M. Moriya⁶, H. Muraishi¹³, Y. Muraki¹¹,
T. Naito⁷, T. Nakase¹⁴, K. Nishijima¹⁴, M. Ohishi¹, J.R. Patterson¹⁵, K. Sakurazawa⁶,
R. Suzuki¹, D.L. Swaby¹⁵, K. Takano⁶, T. Takano⁵, T. Tanimori², F. Tokanai⁵,
K. Tsuchiya¹, H. Tsunoo¹, K. Uruma¹⁴, A. Watanabe⁵, S. Yanagita⁹, T. Yoshida⁹, and
T. Yoshikoshi¹⁶

ABSTRACT

We have observed Markarian 421 in January and March 2001 with the CANGAROO-II imaging Cherenkov telescope during an extraordinarily high state at TeV energies. From 14 hours observations at very large zenith angles,

¹Institute for Cosmic Ray Research, University of Tokyo, Chiba 277-8582, Japan

²Department of Physics, Kyoto University, Kyoto 606-8502, Japan

³MSSSO, Australian National University, ACT 2611, Australia

⁴Institute of Space and Astronautical Science, Kanagawa 229-8510, Japan

⁵Department of Physics, Yamagata University, Yamagata 990-8560, Japan

⁶Department of Physics, Tokyo Institute of Technology, Tokyo 152-8551, Japan

⁷Faculty of Management Information, Yamanashi Gakuin University, Yamanashi 400-8575, Japan

⁸Department of Physics, Konan University, Hyogo 658-8501, Japan

⁹Faculty of Science, Ibaraki University, Ibaraki 310-8512, Japan

¹⁰Faculty of Engineering, Shinshu University, Nagano 380-8553, Japan

¹¹STE Laboratory, Nagoya University, Aichi 464-8601, Japan

¹²National Astronomical Observatory of Japan, Tokyo 181-8588, Japan

¹³Ibaraki Prefectural University of Health Sciences, Ibaraki 300-0394, Japan

¹⁴Department of Physics, Tokai University, Kanagawa 259-1292, Japan

¹⁵Department of Physics and Math. Physics, University of Adelaide, SA 5005, Australia

¹⁶Department of Physics, Osaka City University, Osaka 558-858, Japan

$\sim 70^\circ$, a signal of 298 ± 52 gamma-ray-like events (5.7σ) was detected at $E > 10$ TeV, where a higher sensitivity is achieved than those of usual observations near the zenith, owing to a greatly increased collecting area. Under the assumption of an intrinsic power-law spectrum, we derived a differential energy spectrum $dN/dE = (3.3 \pm 0.9_{stat.} \pm 0.3_{syst.}) \times 10^{-13} (E/10 \text{ TeV})^{-(4.0^{+0.9}_{-0.6}{}_{stat.} \pm 0.3_{syst.})}$ ph./cm²/sec/TeV, which is steeper than those previously measured around 1 TeV, and supports the evidence for a cutoff in the spectrum of Markarian 421. However, the 4σ excess at energies greater than 20 TeV in our data favors a cutoff energy of ~ 8 TeV, at the upper end of the range previously reported from measurements at TeV energies.

Subject headings: BL Lacertae objects: individual (Markarian 421) – gamma rays: observations

1. Introduction

Markarian 421 (Mrk 421, J1104+3812) is a nearby BL Lacertae object ($z = 0.031$) and was the first extragalactic TeV gamma-ray source discovered (Punch et al. 1992). The TeV gamma-ray flux is variable, with flaring behavior observed on time-scales of less than an hour (Gaidos et al. 1996). Extensive measurements have been performed by several experimental groups based on the imaging Cherenkov technique (Aharonian et al. 1999a; Krennrich et al. 1999; Piron et al. 2001). Multi-wavelength observations support the Synchrotron–Self–Compton (SSC) mechanism for the production of TeV gamma-rays from this source (see, e.g., Takahashi et al. 2000; Krawczynski et al. 2001).

TeV gamma-rays from extra-galactic sources suffer absorption due to photon-photon interactions with the inter-galactic infrared background radiation (Nikishov 1962; Gould & Schröder 1967; Stecker, de Jager & Salamon 1992). According to recent measurements of the infrared background (see, e.g., Hauser & Dwek 2001, and references therein) and predictions of the optical depth for TeV gamma-rays (Primack et al. 1999; de Jager & Stecker 2001; Totani & Takeuchi 2002), gamma-rays at energies above 10 TeV from Mrk 421 are expected to be suppressed, since they interact with mid- to far-infrared photons of $\sim 100 \mu\text{m}$.

Mrk 421 became active in 2000 and 2001, especially at the beginning of 2001 (Börst, Götting & Remillard 2001). During this period, northern hemisphere observers measured the energy spectrum with good statistics in the region from several hundred GeV to ~ 10 TeV and reported cutoffs at 3–6 TeV (Krennrich et al. 2001; Aharonian et al. 2002). The cutoff energy is consistent with, or slightly smaller than, that measured for Mrk 501 during its

flaring state in 1997 (Aharonian et al. 1999b, 2001). As Mrk 501 has a similar redshift ($z = 0.034$) to Mrk 421, this suggests the cutoffs may be due to infrared absorption of TeV gamma-rays.

We observed Mrk 421 during the 2001 high state with the CANGAROO-II 10 meter telescope, at very large zenith angles of $\sim 70^\circ$. Similar observations have been reported by the Durham group for Mrk 501 in the high state of 1997 (Chadwick et al. 1999). For these observations, an effective collecting area ~ 10 times larger than that for observations near the zenith is obtained, with an accompanying increase in the gamma-ray energy threshold to ~ 10 TeV.

2. Observations and Analysis

The observations were made with the CANGAROO-II 10 meter telescope (Mori et al. 2001; Tanimori 2001), located near Woomera, South Australia, Australia ($136^\circ 47'E$, $31^\circ 06'S$). The telescope consists of 114 segmented optical mirrors, each of 80 cm diameter (Kawachi et al. 2001). The camera contains 552 half-inch photomultiplier tubes, arranged at $0^\circ.115$ intervals, and covering a field of view of $\sim 3^\circ$.

Mrk 421 was observed for ten nights in early 2001; January 24, 26, 27, 30, 31 and February 1, and March 1–4 (all dates in UT), when the source was extremely active. From the CANGAROO-II telescope site, Mrk 421 culminates at a zenith angle of $69^\circ.3$. Approximately two hours observations were made per night. OFF source data were taken with the right ascension suitably offset. An event trigger was registered when 3 individual pixels exceeded a threshold of ~ 2.5 photoelectrons. After rejecting data affected by clouds and those at zenith angles greater than $71^\circ.5$, 14.34 hours ON source data and 16.65 hours OFF source data remain. A software trigger was applied in order to reduce the effect of pixels randomly triggered by the night sky background. Pixels with pulse-heights of greater than ~ 3.3 photoelectrons, pixel trigger times within 40 nanoseconds of the central value for the event, and three or more adjacent pixels were required. Finally, four or more pixels surviving these cuts were required in each event.

Large zenith angle observations are well-suited to searching for gamma-ray signals at higher energies, as a much larger effective area can be achieved compared to observations near the zenith (Sommers & Elbert 1987; Tanimori et al. 1994), though with a higher energy threshold. From Monte Carlo simulations (Okumura et al. 2001; Enomoto et al. 2002a), an effective area of $\sim 5 \times 10^9$ cm² at $E = 20$ TeV was estimated for observations at 70° , with the area increasing to $\sim 10^{10}$ cm² for higher energies. A threshold energy (where

the gamma-ray detection rate is maximized) of ~ 11 TeV was derived for a $E^{-3.0}$ spectrum. This is an increase by a factor of ~ 30 in comparison with observations near zenith. The energy threshold changes by $\sim \pm 1$ TeV if the spectral index is varied by ± 0.5 .

The selection of the gamma-ray events is based on the parameterization of the elongated shape of the Cherenkov light image using the standard parameters: *width*, *length* (shape), *distance* (location), *asymmetry* (direction), and *alpha* (orientation angle) (Hillas 1982; Punch 1993; Reynolds et al. 1993). Instead of the conventional parameterization cuts, we adopted the Likelihood method (Enomoto et al. 2002a,b), which has a higher efficiency of gamma-ray discrimination than the conventional parameterization technique. The likelihood method uses a single parameter, $R_{prob} = Prob(\gamma)/[Prob(\gamma) + Prob(B.G.)]$, where $Prob(\gamma)$ and $Prob(B.G.)$ are the probabilities for the event having been initiated by a gamma-ray from the source or a background event, respectively. They are the products of individual probabilities for *width*, *length*, and *asymmetry*, which are derived from the probability density functions, including the energy dependence. These functions were obtained using gamma-ray simulations for the signal and the observed OFF source events for the background. R_{prob} ranges from 0 to 1, and the probability of a gamma-ray origin for an event increases as R_{prob} becomes closer to 1, though the gamma-ray acceptance does not significantly decrease in the range of $R_{prob} \lesssim 0.5$. We adopted a relatively loose cut of $R_{prob} > 0.4$ with an additional requirement of $0^\circ.2 < distance < 1^\circ.1$. With these cuts and a further cut excluding events with $alpha \geq 20^\circ$, 86 % of background events are rejected while 63 % of gamma-ray events are expected to be retained.

The resulting event distribution of *alpha* is shown in Figure 1 (a) (left panel). A clear excess over the background is apparent around the source direction. The excess is broadly distributed, up to $\sim 30^\circ$, due to the deterioration of the pointing resolution, caused by the shrinkage of the gamma-ray shower image. This spread in *alpha* distribution is consistent with simulations, as shown in the bottom panel of Figure 1. The OFF source distribution was normalized to that of the ON source by the ratio of the number of the events in $alpha > 40^\circ$ (0.88), which is consistent with the ratio of observation times (0.86), within statistical errors. An excess of 298 ± 52 events, with a significance of 5.7σ (calculated using the method of Li & Ma (1983)) was obtained in the region of $alpha < 20^\circ$. For the confirmation of the detected signal, the conventional parameterization cuts of $0^\circ.2 < distance < 1^\circ.1$, $0^\circ.06 < length < 0^\circ.18$, and $0^\circ.03 < width < 0^\circ.14$ were applied to the data, and a signal of 286 ± 55 events was obtained with 5.2σ significance.

Since the observations were undertaken at large zenith angles, $\sim 70^\circ$, we carefully examined the data and the simulations in more detail:

1. The shrinkage of the shower image, which is problematic for large angle observations,

was studied by a comparison between simulations and data using the background events due to cosmic-ray hadrons. Figure 2 shows the imaging parameters *length* and *width*, observed at large ($\sim 70^\circ$) and small ($\sim 15^\circ$) zenith angles, respectively. The hadron simulations were made using the CORSIKA code (version 6.004) (Heck et al. 1998), considering the cosmic-ray abundance in the TeV region (Mohanty et al. 1998). The resultant distributions of the simulations agree with the data for both small and large angles.

It is also noted that our high resolution imaging camera, which has a pixel spacing size of 0.115° , helped to separate the smaller images of gamma-ray events from those of background events. The expected *length* and *width* distributions of the gamma-ray events, simulated with the spacing size of $0^\circ.115$ and $0^\circ.230$, are shown in the bottom panels of Figure 2. With the larger pixel size, the reconstructed image size increases and becomes more similar to those of hadrons, with an estimated $\sim 50\%$ decrease in the separation efficiency. Although gamma-ray detection is still possible with the larger spacing, the higher resolution imaging camera is more advantageous for large zenith angle observations.

2. The *distance* distribution of the gamma-ray selected events was compared to those from simulations. The location of Cherenkov images due to gamma-ray cascades in the field of view has a particular distribution, while those due to hadron showers are uniformly distributed. For large zenith angle observations in particular, as the observed distances of gamma-ray shower images decrease, there is a substantial difference with the background distribution. Figure 3 shows the *distance* distribution of the gamma-ray selected events, which is obtained by subtracting the OFF source distribution from the ON source distribution after the likelihood and *alpha* cuts were applied. The resulting distribution has a clear peak around $0^\circ.7$ from the source direction, which agrees reasonably well with simulations and differs from that of the cosmic ray background, which provides additional confirmation of the detection of TeV gamma-rays.

3. The “standard candle” at TeV energies, the Crab nebula, was observed at relatively large zenith angles of $\sim 55^\circ$ in November and December 2000, and the gamma-ray flux was measured for the confirmation of the analysis method and the estimation of the systematic error in the energy scale. Using the same analysis technique as that used for Mrk 421, the differential energy spectrum was derived over the energy range from 2 TeV to ~ 20 TeV (Itoh et al. 2002), which agrees well with other experiments (Tanimori et al. 1998; Aharonian et al. 2000; Krennrich et al. 2001), within a $\sim 15\%$ error in the energy scale.

These consistencies provide robust supporting evidence for the detection of $E > 10$ TeV gamma-rays from Mrk 421.

3. Discussion

Figure 4 (inserted panel) shows the raw energy spectrum of the observed gamma-ray events from Mrk 421. The gamma-ray energy was assigned from the pulse-height sum of the individual pixels, using a relation obtained from the simulations. This method is similar to that described in Mohanty et al. (1998), and an energy resolution of $\sim 31\%$ is estimated. The excess events are distributed in the energy range 7–45 TeV, however one must take care of the spill-over effect from the lower energies due to the finite energy resolution. In order to take this effect into account, simulated gamma-ray spectra, with the spectral indexes and cutoff energies varied, were compared to the data and the observed spectral parameters were determined from the values which minimized the value of χ^2 . With the assumption of a power-law spectrum, the differential flux was fitted by

$$\frac{dN}{dE} = (3.3 \pm 0.9_{stat.} \pm 0.3_{syst.}) \times 10^{-13} \left(\frac{E}{10 \text{ TeV}} \right)^{-(4.0^{+0.9}_{-0.6}{}_{stat.} \pm 0.3_{syst.})} \text{ ph./cm}^2/\text{sec/TeV}$$

with $\chi^2=2.5/2$ *d.o.f.* The cut dependence on R_{prob} and *alpha* parameters, and the trigger conditions in the simulation, were considered as sources of the systematic uncertainties. The systematic errors giving rise to uncertainty in the energy scale such as Cherenkov photon scattering in the atmosphere are not included here, but are considered in more detail later. The derived spectrum is steeper than those observed at lower TeV energies. The spectral shape was tested with a cutoff spectrum of $E^{-1.9} \exp(-E/4\text{TeV})$, as was derived from the measurements by the Whipple and HEGRA-CT groups, with the spectral index being the hardest one observed during the strong flaring period (Aharonian et al. 2002; Krennrich et al. 2002). The fitting result did not improve compared to that with the power-law assumption ($\chi^2=5.0/3$ *d.o.f.*), as an excess of events above 20 TeV is apparent, as shown in Fig 1 (b). An excess of 103 ± 26 (4.0σ) was observed with *alpha* $< 20^\circ$, while 11 events are expected for the cutoff spectrum, based on an estimation using the event ratio between 10–20 TeV and over 20 TeV. However, if a cutoff energy of 8 TeV is assumed, the consistency with the data becomes better (48 events expected for $E^{-1.9} \exp(-E/8\text{TeV})$). This cutoff energy is at the high end of the range allowed for Mrk 501 (Aharonian et al. 1999b, see also Aharonian et al. 2001). Since these two AGNs have similar redshifts, the cutoff energies in both spectra are expected to be similar, assuming the attenuation is predominantly due to infrared absorption. As there is only a 2σ difference between our observations and this prediction, our result falls in the acceptable range of the absorption hypothesis due to the cosmic infrared background.

Figure 4 (main panel) shows the measured energy flux, assuming the power-law spectrum. Data for the Whipple (Krennrich et al. 2001) and HEGRA-CT groups (Aharonian

et al. 2002), observed during a similar period of the flaring state (January–March 2001) are also shown. The observation periods were not exactly the same and the source varied significantly during this high state, therefore the absolute fluxes are expected to differ at some level. The absolute flux level determined from the CANGAROO-II data is within the observed range of the flux variation reported by the Whipple group (Krennrich et al. 2002), and the spectral slope around 10 TeV is consistent with that of these two groups, supporting the roll-over from the flatter spectrum measured at lower energies.

For large zenith angle observations, a large uncertainty in the energy scale, due to the absorption of Cherenkov photons in the atmosphere, is inevitable. Only Rayleigh scattering was considered in the simulation code to avoid over-estimating the gamma-ray energies. The inclusion of Mie scattering and ozone absorption would affect the energy scale by $\sim 30\%$ and $\sim 3\%$, respectively, based on numerical estimations using the program code of Kneizys et al. (1996). We stress that these effects increase the energy scale. The use of the “flat-Earth” approximation for the atmosphere in the simulations requires a $\sim 6\%$ correction which has already been taken into account in the discussion above.

The measurement of spectra at large zenith angles was verified by observations of the Crab nebula up to the zenith angles of $\sim 55^\circ$, although calibration using the Crab nebula at the same zenith angles as the Mrk 421 observations ($\sim 70^\circ$) is unfortunately impractical with the current instrumental sensitivity. The strong gamma-ray emission of Mrk 421 (~ 3 times that of Crab nebula) enabled us to detect the source in only 14 hours. In order to detect the Crab nebula at the same significance level, more than 150 hours observations would be required.

In summary, owing to the large effective area and the high resolution performance of the Cherenkov imaging camera, $E > 10$ TeV gamma-rays from Mrk 421 were detected at a high confidence level at zenith angles of $\sim 70^\circ$ with 14 hours of observations. The derived spectrum in the region of 10–30 TeV is steeper than that around 1 TeV, which supports the cutoff spectrum of Mrk 421 measured in the 0.2–10 TeV range by other groups. The excess observed above 20 TeV is strongly suggestive of a higher cutoff energy, ~ 8 TeV, compared to the lower energy observations. These observations confirm, with the support of detailed simulations, the viability of the large zenith angle technique. Large zenith angle observations provide a unique method of measuring the spectrum in the important energy range above 10 TeV with a relatively short observation time.

The authors thank F. Krennrich and D. Horns for kindly providing flux data. This project is supported by a Grant-in-Aid for Scientific Research of Ministry of Education, Culture, Science, Sports and technology of Japan and Australian Research Council. The

receipt of JSPS Research Fellowships is also acknowledged. We thank the DSC Woomera for their assistance in constructing the telescope.

REFERENCES

- Aharonian, F. A. et al. 1999a, *A&A* 350, 757
- Aharonian, F. A. et al. 1999b, *A&A* 349, 11
- Aharonian, F. A. et al. 2000, *ApJ* 539, 317
- Aharonian, F. A. et al. 2001, *A&A* 366, 62
- Aharonian, F. A. et al. 2002, *A&A* submitted, preprint (astro-ph/0205499)
- Börst, H. G., Götting, N & Remillard, R 2001, *IAU Circ.* 7568
- Chadwick, P. M. et al. 1999, *J. Phys. G:Nucl. Phys.* 25, 1749
- de Jager, O. C. & Stecker, F. W. 2002, *ApJ* 566, 738
- Enomoto, R. et al. 2002a, *Astropart. Phys.* 16, 235
- Enomoto, R. et al. 2002b, *Nature* 416, 823
- Gaidos, J. A. et al. 1996, *Nature* 383, 319
- Gould, R. J. & Schröder, G. 1967, *Phys. Rev.* 155, 1408
- Hauser, M. G. & Dwek, E. 2001, *ARA&A* 39, 249
- Heck, D. et al. 1998, *Forschungszentrum Karlsruhe Report FZKA 6019*
- Hillas, A. M. 1982, *J. Phys. G* 8, 1475
- Itoh, C. et al. 2002, in preparation
- Kawachi, A. et al. 2001, *Astropart. Phys.* 14, 261
- Kneizys, F. K. et al. 1996, MA 01731, Hanscom AFB, Phillips Laboratory
- Krawczynski, H. et al. 2001, *ApJ* 559, 187
- Krennrich, F. et al. 1999, *ApJ* 511, 149

- Krennrich, F. et al. 2001, ApJ 560, L45
- Krennrich, F. et al. 2002, ApJ 575, L9
- Li, T. & Ma, Y. 1983, ApJ 273, 317
- Mohanty, G. et al. 1998, Astropart. Phys. 9, 15
- Mori, M. et al. 2001, Proc. 27th Int. Cosmic Ray Conf. (Hamburg) 5, 2831
- Nikishov, A. I. 1962, Sov. Phys. JETP 14, 393
- Okumura, K. et al. 2001, Proc. 27th Int. Cosmic Ray Conf. (Hamburg) 7, 2679
- Piron, F. et al. 2001, A&A 374, 895
- Primack, J. R. et al. 1999, Astropart. Phys. 11, 93
- Punch, M. et al. 1992, Nature 358, 477
- Punch, M. 1993, Ph.D. thesis, National University of Ireland
- Reynolds, P. T. et al. 1993, ApJ 404, 206
- Sommers, P. & Elbert, J.W. 1987, J. Phys. G: Nucl. Phys. 13, 553
- Stecker, F. W., de Jager, O.C., Salamon, M.H. 1992, ApJ 390, L49
- Takahashi, T. et al. 2000, ApJ 542, L105
- Tanimori, T. et al. 1994, ApJ 429, L61
- Tanimori, T. et al. 1998, ApJ 487, L65
- Tanimori, T. 2001, Prog. Theor. Phys. Suppl. 143, 78
- Totani, T. & Takeuchi, T. 2002, ApJ 570, 470

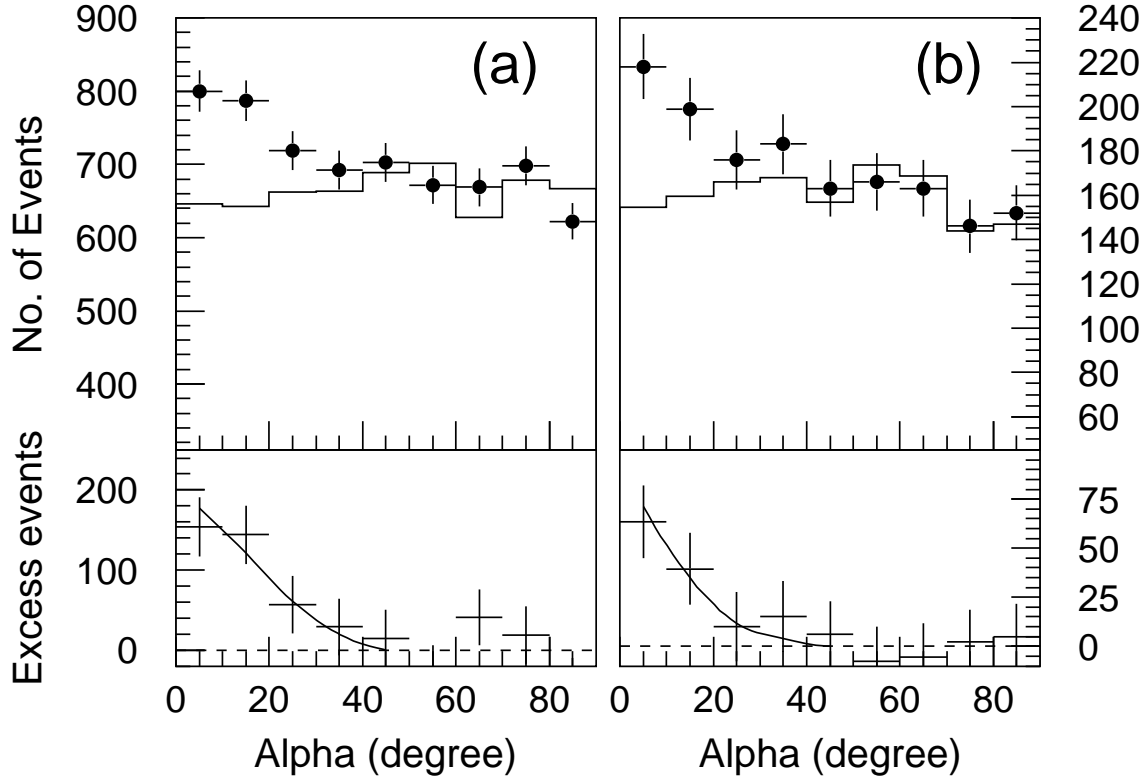


Fig. 1.— Image orientation angle (α) distributions for gamma-ray-like events with respect to the direction to Markarian 421. The left figure (a) shows the distributions for all energies, and the right figure (b) for those with reconstructed energies above 20 TeV. In the upper panel, filled circles with error bars (statistical only) and solid lines are for the ON and OFF source data, respectively. The lower panel shows the excess events of the ON source above the background (OFF source) level. The solid curves show the expected spread of gamma-ray events in the α distribution from simulations.

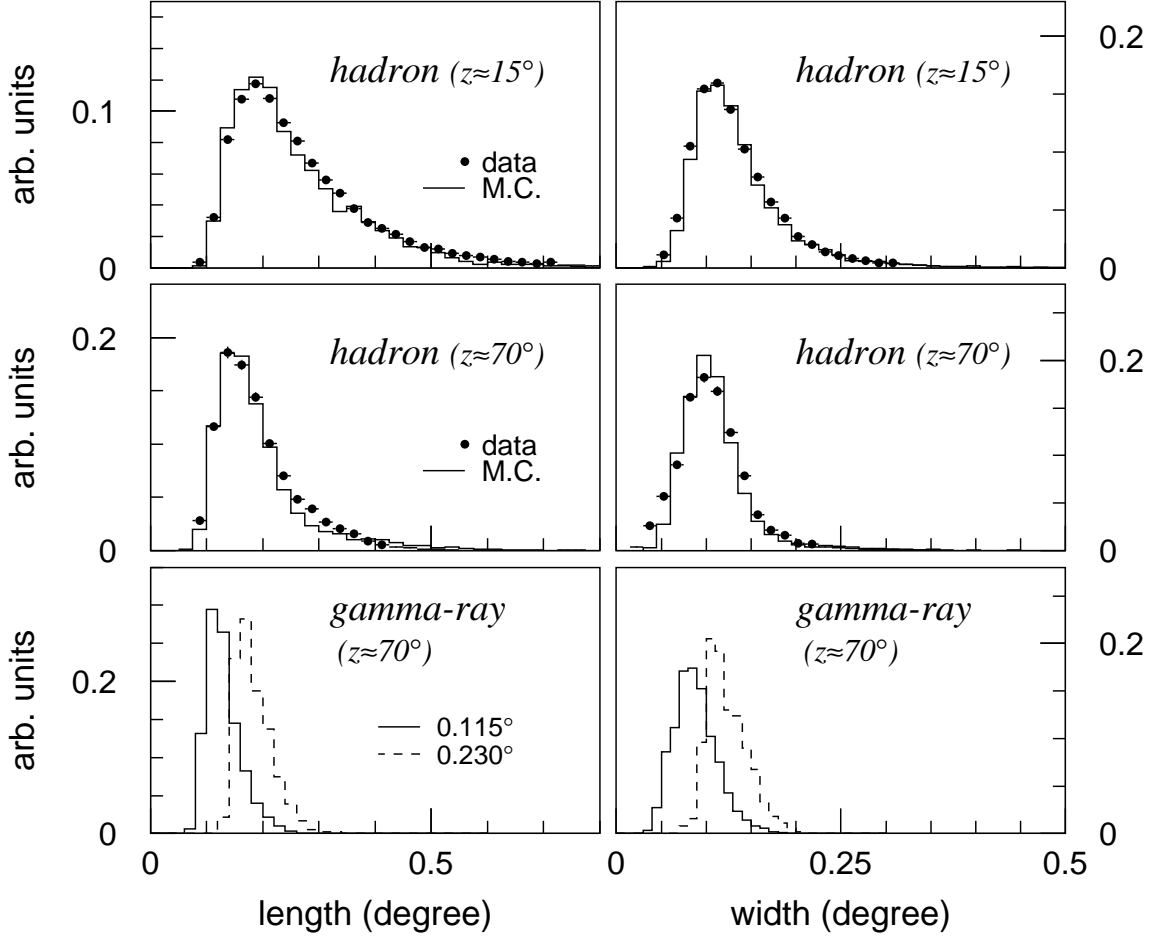


Fig. 2.— Distributions of the image-centroid parameters (*length* and *width*) observed at the large ($\sim 70^\circ$) and small ($\sim 15^\circ$) zenith angles. In the upper and middle panels, the observed background data (dots with error bars) and hadrons simulations (solid lines) are shown for the large and small angles. In the bottom panels, those of the gamma-ray simulations, with different camera pixel spacings (0.115° and 0.230°), are shown for large angle observations.

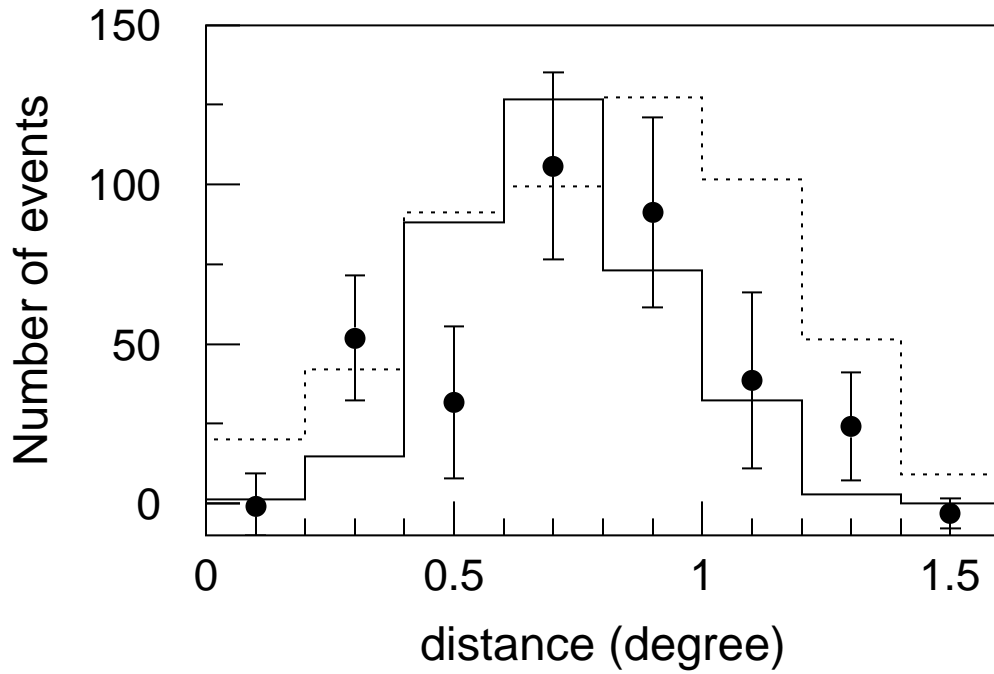


Fig. 3.— Distributions of the image shape parameter *distance*, after subtracting normalized OFF-source data from ON-source data (circles with error bars), gamma-ray simulation (solid line) and hadron background (dotted line).

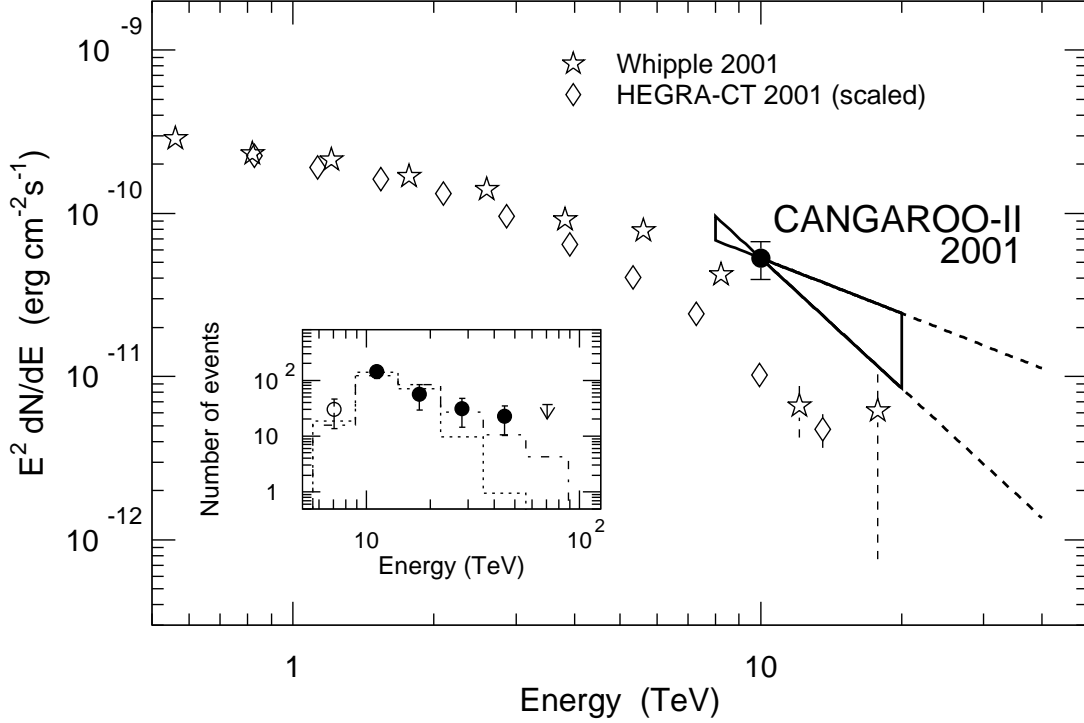


Fig. 4.— The observed gamma-ray fluxes (main panel) and the energy spectrum of gamma-ray events (inserted panel). In the inserted panel, data are represented by circles with error bars, with a 2σ upper limit plotted at the highest energy. Best-fit spectra for a power-law ($E^{-4.0}$; dot-dashed line) and a cut-off ($E^{-1.9} \exp(-E/4 \text{ TeV})$; dotted line) are shown (see text for details). The data shown with the filled circles were used for the spectral shape fitting. In the main panel, the measured flux under the assumption of a power-law spectrum is shown with error bars and the area corresponding to statistical errors of $\pm 1\sigma$. Whipple (Krennrich et al. 2001) and HEGRA-CT (Aharonian et al. 2002) spectra measured in similar periods are also shown. The fluxes plotted for the HEGRA-CT group have been scaled in order to normalize it to the Whipple flux at 1 TeV.